metals

MDPI

Article

Gas Metal Arc Welding Using Novel CaO-Added Mg Alloy Filler Wire

Minjung Kang, Youngnam Ahn and Cheolhee Kim *

Joining R & D Group, Korea Institute of Industrial Technology, 156 Gaetbeol-ro (Songdo-dong), Yeonsu-Gu, Incheon 21999, Korea; kmj1415@kitech.re.kr (M.K.); welidng@kitech.re.kr (Y.A.)

* Correspondence: chkim@kitech.re.kr; Tel.: +82-32-850-0222

Academic Editor: Giuseppe Casalino
Received: 25 February 2016; Accepted: 23 June 2016; Published: 8 July 2016

Abstract: Novel "ECO Mg" alloys, i.e., CaO-added Mg alloys, which exhibit oxidation resistance during melting and casting processes, even without the use of beryllium or toxic protection gases such as SF_6, have recently been introduced. Research on ECO Mg alloys is still continuing, and their application as welding filler metals was investigated in this study. Mechanical and metallurgical aspects of the weldments were analysed after welding, and welding behaviours such as fume generation and droplet transfer were observed during welding. The tensile strength of welds was slightly increased by adding CaO to the filler metal, which resulted from the decreased grain size in the weld metal. When welding Mg alloys, fumes have been unavoidable so far because of the low boiling temperature of Mg. Fume reduction was successfully demonstrated with a wire composed of the novel ECO Mg filler. In addition, stable droplet transfer was observed and spatter suppression could be expected by using CaO-added Mg filler wire.

Keywords: magnesium; fusion welding; CaO-added filler; fumes; microstructure

1. Introduction

Weight reduction is becoming an increasingly important issue in the automotive industry, to adhere to global CO_2 emission and fuel consumption regulations. Magnesium alloys are a promising lightweight alternative to aluminium alloys and high-strength steel in the automotive industry. Although Mg alloys have many advantages such as high specific strength, low density, and good casting ability, they are inherently reactive during processing of the molten Mg alloy; therefore, sulphur hexafluoride (SF_6) protection gas must be used or beryllium must be added to the Mg alloy to prevent ignition. Recently, so-called "ECO Mg" alloys have been invented by introducing CaO to the conventional Mg alloys. Previous studies have reported that Mg oxidation and ignition could be controlled and minimized in various ECO Mg alloys during melting [1–4], and improved mechanical properties and metallurgical characteristics have been reported [5–7].

Welding and joining are essential processes to manufacture automotive parts, and several welding processes have been proposed for Mg alloys. However, welding Mg alloys is inherently difficult because of their material characteristics such as low boiling temperatures, a high thermal expansion coefficient, and high thermal conductivity. Friction stir welding, a solid-state process, has been suggested to overcome the disadvantages of Mg alloys [8–11]. Also, numerous research studies for fusion welding processes that are more familiar and flexible have been recently published to optimize the fusion welding processes. These include gas tungsten arc welding [12,13], gas metal arc welding (GMAW) [14], and laser welding [15,16]. Recent studies on friction stir welding of ECO Mg alloy revealed that the mechanical and metallurgical characteristics of friction stir welds were also improved by the enhanced mechanical properties of ECO Mg alloy [17,18]. Other interesting results come from the laser welding of ECO Mg alloy. In addition to improved mechanical and metallurgical characteristics, laser-induced plasma can be controlled using ECO Mg alloy, which can prevent plasma interference with laser irradiation and can consequently lead to increased welding speed to realize fully penetrated welds [19].

In GMAW, the filler metal electrode has two important roles: as an electrode and as the source of deposited metal in the welds. The filler wire, which is normally employed as the positive pole, is exposed to the high-temperature welding arc, and electrons are condensed into the filler wire. Thus, the molten drop hanging on the end of the filler wire is easily overheated. Mg in the filler wire can result in droplet evaporation due to its low boiling point. However, most previous studies of droplet evaporation and fume generation have focused on Mg-containing Al filler wires [20–23] and only spatter generation and porosity in Mg filler wire were discussed [14]. On the other hand, as the source of deposited metal in welds, ECO Mg filler wire dissolved in the weld metal can improve mechanical and metallurgical characteristics as confirmed in autogenous laser welding of ECO Mg alloy [19].

In this study, ECO Mg alloy was employed as a filler metal for GMAW, and the weldability was studied. First, various mechanical and metallurgical characteristics of welds are explained, and then welding phenomena such as fume generation and droplet transfer monitored during GMAW will be discussed.

2. Experimental Setup

In this study, the base material was a commercial AZ 31 alloy sheet with a measured tensile strength of 278 MPa whose measured chemical composition is given in Table 1. The sheet was 150 mm long, 120 mm wide, and 1.5 mm thick. Before welding, the oxide film on the specimen was removed with a stainless brush in the area intended for welding.

Table 1. Chemical composition of base material (wt. %).

Al	Zn	Mn	Si	Fe	Cr	Mg
3.098	0.981	0.304	0.037	0.013	0.013	Bal.

The filler materials were a commercial AZ 31 alloy (AZ31-A) and CaO-added AZ 31 alloy (AZ31-B). Both fillers were 1.2 mm in diameter, and their chemical compositions measured by ICP are given in Table 2.

Table 2. Chemical compositions of filler wires (wt. %).

Filler Wire	Al	Zn	Mn	Si	Ca	Mg
AZ31-A	2.76	0.92	0.40	0.019	-	Bal.
AZ31-B	3.10	0.63	0.19	1.18	0.89	Bal.

In the welding experiments, bead-on-plate (BOP) welding was conducted and the fillers were fed into the weld pool with a lead angle of 20° from perpendicular, as shown in Figure 1a. Figure 2 shows the arc welding system with a six-axis articulate robot, a wire feeding system, and a welding power source. Argon shielding gas was supplied by a welding torch with a flow rate of 20 L/min. Mg alloys have a low boiling temperature, and a tremendous amount of spatters are generated when welding in the standard mode [14]. To avoid spatter generation and minimize heat input during welding, a Fronius CMT (cold-metal-transfer) 3200 was used as the power source, operating in the CMT mode, which is a type of short circuit transfer mode welding. The welding current, welding voltage, wire feed speed, and welding speed selected were 80 A, 10.2 V, 6.4 m/min, and 0.6 m/min, respectively.

After welding, the metallurgical and mechanical characteristics of the welds were examined. The specimens were polished and etched for 50 s in a solution of 2 mL hydrochloric acid and 100 mL ethanol in order to observe the microstructure of welds using a light microscope. Static tensile tests with a test speed of 5 mm/min were conducted on the specimen shown in Figure 3a according to ISO 6892-1:2009. The specimens were prepared with and without the weld reinforcements in Figure 3b,c. Mechanical machining was used to remove the weld reinforcement. The micro-Vickers hardness was measured at 0.3 mm intervals in the welds under a load of 0.49 N (50 gf) and a holding time of 10 s.

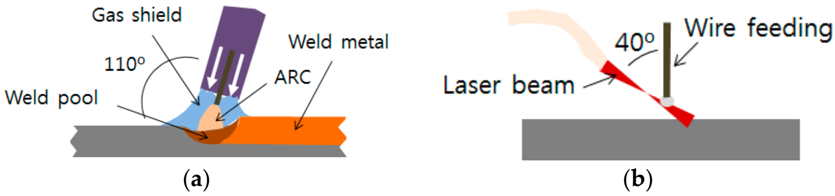

Figure 1. Setup for experiments: (**a**) Gas metal arc welding; (**b**) Laser melting.

Figure 2. Picture of the arc welding system used.

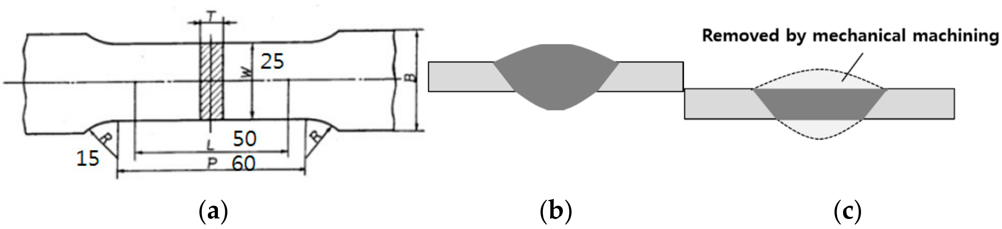

Figure 3. Schematic diagrams of prepared tensile test specimen (all dimensions in mm). (**a**) *X-Y* plane; (**b**) *X-Z* plane section with reinforcement; (**c**) *X-Z* plane section without reinforcement.

In the fume generation experiments, GMAW and laser melting experiments were conducted. The setup for GMAW was the same as for welding, and two welding modes—the CMT and pulse welding modes—were employed. In the CMT mode welding, the welding conditions were identical to the previous welding experiments. In the pulse mode welding, the average welding current, welding voltage, wire feed speed, and welding speed were 82 A, 22.4 V, 8.7 m/min, and 0.5 m/min, respectively.

During the laser melting experiment, as shown in Figure 1b, the filler wires were fed perpendicularly to the specimen with a wire feed speed of 3 m/min. The laser beam with a power of 4 kW was delivered using a 200-µm-diameter optical fibre (LLK-D 02, Trumpf Laser- und Systemtechnik GmbH, Ditzingen, Germany) from a Yb:YAG disk laser source (Trumpf HLD 4002, Trumpf Laser- und Systemtechnik GmbH, Ditzingen, Germany) and irradiated the end of the filler wire at an inclination angle of 40° and a defocusing distance of 3 mm.

High-speed photography using a Photron FASTCAM Ultima APX camera was employed with a capture speed of 2000 frames per second to record fume generation behaviour. A neutral density filter (ND400) and metal-halide back lighting were used to obtain clear images.

3. Welding Characteristics

Figure 4 shows the bead appearance and cross-section for welds with each of the filler wires. Sound bead appearance and cross-section were achieved for both fillers under the given welding conditions. Tensile tests were carried out for specimens with and without weld reinforcement. Joint efficiency was defined as the ratio of average tensile strength of the weldment to that of the base material, and is given in Figure 5. The specimens with weld reinforcement were fractured at the heat-affected zone, whereas those without weld reinforcement were fractured at the weld metal as shown in Figure 6. The fracture location did not vary with the filler wire. However, the tensile strengths of weldments welded with the CaO-containing AZ31-B wire were slightly higher than those welded with the conventional AZ31-A wire.

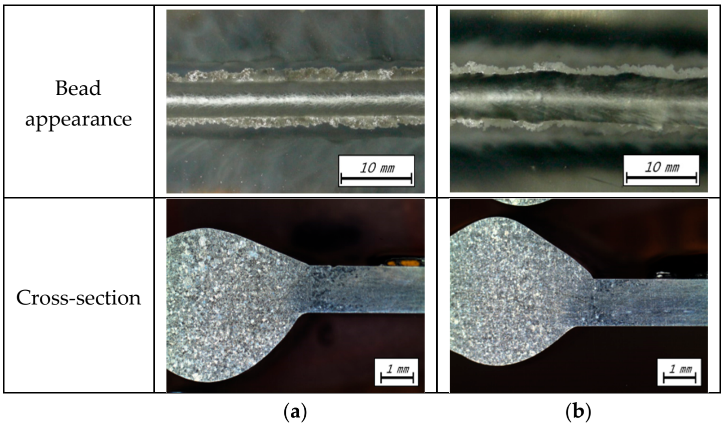

Figure 4. Bead shapes for bead-on-plate (BOP) welding: (**a**) AZ31-A; (**b**) AZ31-B.

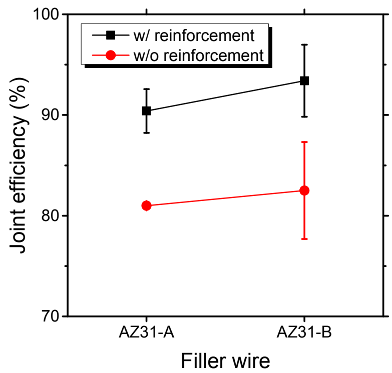

Figure 5. Joint efficiency for BOP welding.

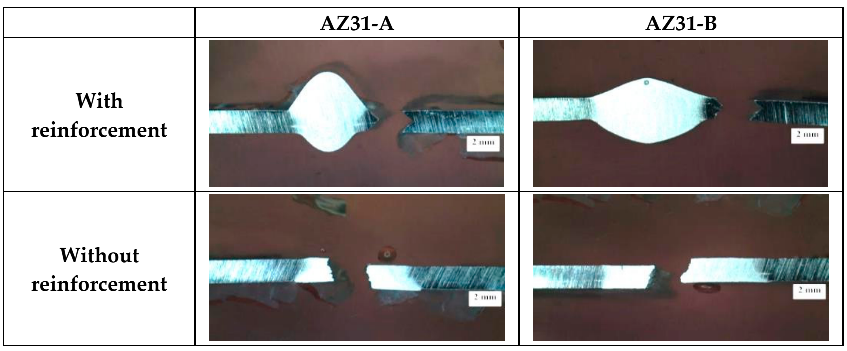

Figure 6. Fractured specimen with and without reinforcement by tensile test.

Figures 7 and 8 show the hardness profiles and microstructures, respectively, of the weldments. The increase in the hardness of the weld metal with the AZ31-B wire is clearly observed, while the hardness of the weld metal with the AZ31-A wire is even lower than that of the base metal. A previous study explained that the increase in hardness results from the Al_2Ca intermetallic compound in the CaO-containing Mg alloy [2]. The microstructure of the base metal and the heat-affected zone were identical because only the filler metal varied. In the heat-affected zone, abnormal grain growth was observed due to the heat input during welding. Grain size in the weldment—even those containing CaO—is larger than that of the base material fabricated by hot rolling, which leads to dynamic recrystallisation due to intense plastic deformation [24]. The grains found for the weldment with the AZ31-B wire were finer than those for the AZ31-A wire. The previous research (Reference [5]) demonstrated that grain refining was driven by the secondary phase, Al_2Ca. In Figure 8c,d, the grain size in the weld metal was measured by using ISO 643:2003. The measured values are 59.9 μm and 20.4 μm for the weld metals with AZ31-A and AZ31-B, respectively, which can explain the difference in the hardness profile in the weld metal.

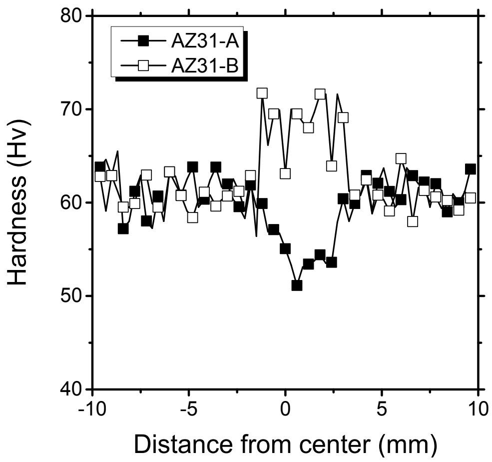

Figure 7. Hardness profile for BOP welding.

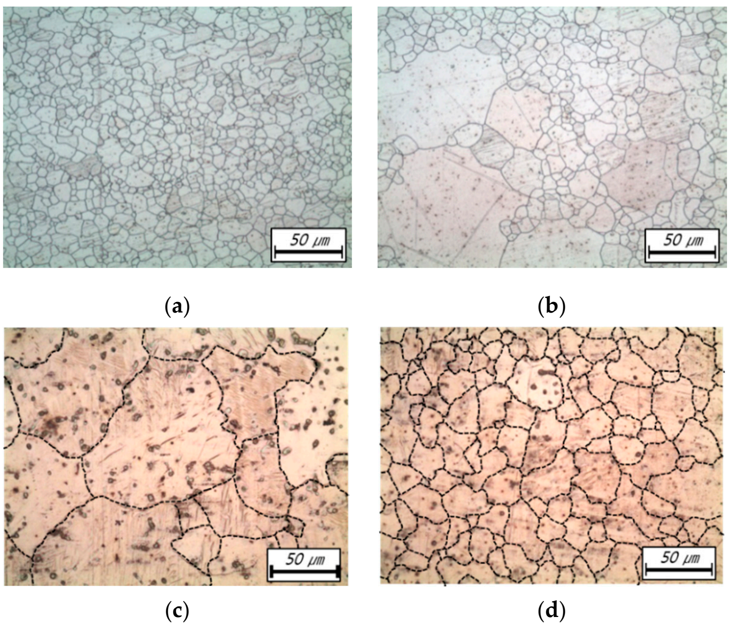

Figure 8. Microstructures of (**a**) base metal (BM); (**b**) heat-affected zone (HAZ); and weld metal (WM) (**c**) AZ31-A; (**d**) AZ31-B.

4. Fume Generation and Droplet Transfer

Figure 9 compares high-speed images taken during the CMT mode welding. Comparing both filler wires shows that fume generation was reduced when the AZ31-B filler wire was used. In the case of the CaO-containing Mg alloy, a thin CaO-rich barrier layer was formed at the surface; this layer can successfully suppress rapid oxidation and burning during the melting process [4]. During welding, the filler wire was melted and a droplet was formed at the end of the wire. The burning resistance of the AZ31-B filler wire could result in fume suppression, and this is more clearly confirmed during the laser melting experiment, as shown in Figure 10. The welding fumes can be generated from either the molten droplet or the weld pool [25], but no fumes were generated from the weld pool in the laser melting experiment.

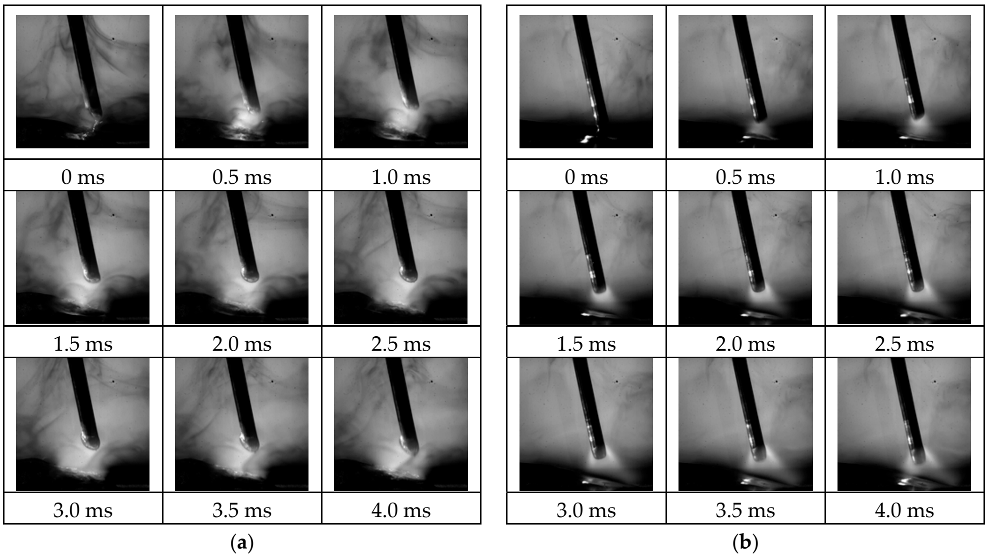

Figure 9. High-speed images during the cold-metal-transfer mode welding: (**a**) AZ31-A; (**b**) AZ31-B.

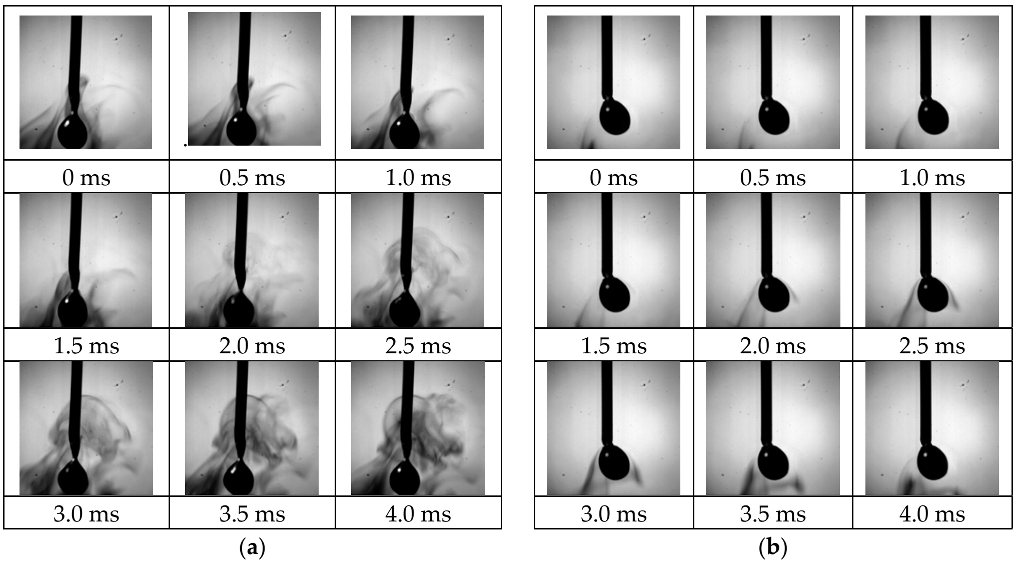

Figure 10. High-speed images during laser melting: (**a**) AZ31-A; (**b**) AZ31-B.

Pulse mode welding was conducted to implement relatively high-current welding. Figure 11 shows the high-speed images obtained during pulse mode welding. During the pulse mode welding, fume suppression by the AZ31-B wire was not clearly observed because of the high welding current.

However, the taper was formed at the end of the wire and the pinch force to detach the droplet increased, which can enhance spray transfer [26]. Therefore, the droplet transfer mode changed from globular transfer to spray transfer mode in which droplet size was reduced and the droplets were more rapidly transferred into the weld pool. In the conventional GMAW of Mg alloys, a large droplet hanging on the wire can be expelled by sudden arc expansion which causes severe spattering [14]. Small droplet size and fast transfer time would be helpful to suppress spatter generation in welding Mg alloys.

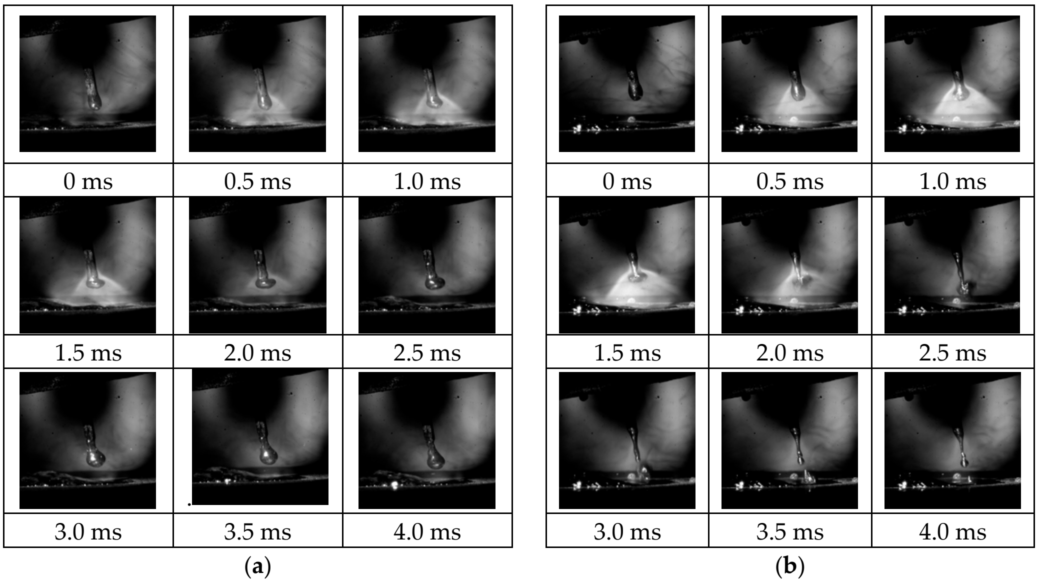

Figure 11. High-speed images during the pulse mode welding: (**a**) AZ31-A; (**b**) AZ31-B.

5. Conclusions

In this study, welding characteristics, fume generation, and droplet transfer behaviour of the CaO-added AZ31 filler wire were compared with the conventional AZ31 filler wire. The conclusions are as follows:

(1) The tensile strength of weldments was slightly increased by using the CaO-added AZ31 filler wire. By adding CaO, the grain size in the weld metal decreased from 59.9 μm to 20.4 μm, and the average hardness in the weld metal increased from 55.3 Hv to 68.9 Hv.

(2) Welding fumes were successfully suppressed during the CMT mode welding. The fume suppression was due to the burning resistance of CaO-added Mg alloy, and this has been confirmed by using the laser melting test.

(3) In the pulse mode welding, spray transfer mode welding was achieved, which enabled stable droplet transfer. Also, the suppression of spatter was expected because of the small droplet size and fast transfer time.

Author Contributions: M. Kang and Y. Ahn performed the experiments; M. Kang and C. Kim wrote the paper.

Conflicts of Interest: The authors declare no conflicts of interest.

References

1. Lee, J.K.; Yoon, Y.O.; Kim, S.K. Development of environment-friendly CaO added AZ31 Mg alloy. *Solid State Phenom.* **2007**, *124*, 1481–1484. [CrossRef]
2. Ha, S.-H.; Lee, J.-K.; Kim, S.K. Effect of CaO on oxidation resistance and microstructure of pure Mg. *Mater. Trans.* **2008**, *49*, 1081–1083. [CrossRef]

3. Lee, J.-K.; Kim, S.K. Effect of CaO composition on oxidation and burning behaviors of AM50 Mg alloy. *Trans. Nonferrous Met. Soc. China* **2011**, *21*, 23–27. [CrossRef]
4. Lee, D.B. High temperature oxidation of AZ31 + 0.3 wt. % Ca and AZ31 + 0.3 wt. % CaO magnesium alloys. *Corros. Sci.* **2013**, *70*, 243–251. [CrossRef]
5. Kim, S.K. Design and development of high-performance Eco-Mg alloys. In *Magnesium Alloys-Design, Processing and Properties*; Czerwinski, F., Ed.; InTech: Rijeka, Croatia, 2011; pp. 431–468.
6. Nam, T.H.; Kim, S.H.; Kim, J.G.; Kim, S.K. Corrosion resistance of extruded Mg-3Al-1Zn alloy manufactured by adding CaO for the replacement of the protective gases. *Mater. Corros.* **2014**, *65*, 577–581. [CrossRef]
7. Nam, N.; Bian, M.; Forsyth, M.; Seter, M.; Tan, M.; Shin, K. Effect of calcium oxide on the corrosion behaviour of AZ91 magnesium alloy. *Corros. Sci.* **2012**, *64*, 263–271. [CrossRef]
8. Esparza, J.; Davis, W.; Trillo, E.; Murr, L. Friction-stir welding of magnesium alloy AZ31B. *J. Mater. Sci. Lett.* **2002**, *21*, 917–920. [CrossRef]
9. Park, S.H.C.; Sato, Y.S.; Kokawa, H. Effect of micro-texture on fracture location in friction stir weld of Mg alloy AZ61 during tensile test. *Scr. Mater.* **2003**, *49*, 161–166. [CrossRef]
10. Carlone, P.; Palazzo, G. Characterization of TIG and FSW weldings in cast ZE41A magnesium alloy. *J. Mater. Process. Technol.* **2015**, *215*, 87–94. [CrossRef]
11. Carlone, P.; Astarita, A.; Rubino, F.; Pasquino, N. Microstructural Aspects in FSW and TIG Welding of Cast ZE41A Magnesium Alloy. *Metall. Mate. Trans. B* **2016**, *47*, 1340–1346. [CrossRef]
12. Liu, L.; Dong, C. Gas tungsten-arc filler welding of AZ31 magnesium alloy. *Mater. Lett.* **2006**, *60*, 2194–2197. [CrossRef]
13. Liu, L.-M.; Cai, D.-H.; Zhang, Z.-D. Gas tungsten arc welding of magnesium alloy using activated flux-coated wire. *Scr. Mater.* **2007**, *57*, 695–698. [CrossRef]
14. Wagner, D.; Yang, Y.; Kou, S. Spatter and porosity in gas-metal arc welding of magnesium alloys: Mechanisms and elimination. *Weld. J.* **2013**, *92*, 347–362.
15. Cao, X.; Jahazi, M.; Immarigeon, J.; Wallace, W. A review of laser welding techniques for magnesium alloys. *J. Mater. Process. Technol.* **2006**, *171*, 188–204. [CrossRef]
16. Liu, L.; Wang, J.; Song, G. Hybrid laser—TIG welding, laser beam welding and gas tungsten arc welding of AZ31B magnesium alloy. *Mater. Sci. Eng. A* **2004**, *381*, 129–133.
17. Choi, D.H.; Ahn, B.W.; Kim, S.K.; Yeon, Y.M.; Kim, Y.J.; Park, S.-K.; Jung, S.B. Microstructure evaluation of friction stir welded AZ 91 with CaO Mg alloy. *Mater. Trans.* **2011**, *52*, 802–805. [CrossRef]
18. Choi, D.-H.; Kim, S.-K.; Jung, S.-B. The microstructures and mechanical properties of friction stir welded AZ31 with CaO Mg alloys. *J. Alloy. Compd.* **2013**, *554*, 162–168. [CrossRef]
19. Kang, M.; Kim, C. Effect of CaO contents on Yb:YAG disk laser weldability of AZ31 Mg alloy. *Mater. Sci. Forum* **2015**, *804*, 31–34. [CrossRef]
20. Wang, J.; Nishimura, H.; Katayma, S.; Mizutani, M. Evaporation phenomena of magnesium from droplet at welding wire tip in pulsed MIG arc welding of aluminium alloys. *Sci. Technol. Weld. Join.* **2011**, *16*, 418–425. [CrossRef]
21. Kim, C.-H.; Ahn, Y.-N.; Lee, K.-B. Droplet transfer during conventional gas metal arc and plasma-gas metal arc hybrid welding with Al 5183 filler metal. *Curr. Appl. Phys.* **2012**, *12*, 178–183. [CrossRef]
22. Semenov, I.; Krivtsun, I.; Demchenko, V.; Semenov, A.; Reisgen, U.; Mokrov, O.; Zabirov, A. Modelling of binary alloy (Al-Mg) anode evaporation in arc welding. *Model. Simul. Mater. Sci. Eng.* **2012**, *20*. [CrossRef]
23. Reisgen, U.; Mokrov, O.; Zabirov, A.; Krivtsun, I.; Demchenko, V.; Lisnyi, O.; Semenov, I. Task of volumetrical evaporation and behaviour of droplets in pulsed MIG welding of AlMg alloys. *Weld. World* **2013**, *57*, 507–514. [CrossRef]
24. Fatemi-Varzaneh, S.; Zarei-Hanzaki, A.; Beladi, H. Dynamic recrystallization in AZ31 magnesium alloy. *Mater. Sci. Eng. A* **2007**, *456*, 52–57. [CrossRef]
25. Chae, H.; Kim, C.; Kim, J.; Rhee, S. Fume generation behaviors in short circuit mode during gas metal arc welding and flux cored arc welding. *Mater. Trans.* **2006**, *47*, 1859–1863. [CrossRef]
26. Kim, Y.; Eagar, T. Analysis of metal transfer in gas metal arc welding. *Weld. J.* **1993**, *72*, 269–278.